2022 IEEE 23rd International Workshop on Signal Processing Advances in Wireless Communication (SPAWC) | 978-1-6654-9455-7/22/$31.00 ©2022 IEEE | DOI: 10.1109/SPAWC51304.2022.9833975

Wavefront Engineering at Terahertz Frequencies Through Intelligent Reflecting Surfaces

Arjun Singh*, Ali J. Alqaraghuli†, and Josep M. Jornet†

*Department of Engineering
SUNY Polytechnic Institute, Utica, NY, USA E-mail: singha8@sunypoly.edu

†Department of Electrical and Computer Engineering
Northeastern University, Boston, MA, USA E-mail: {alqaraghuli.a, jmjornet}@northeastern.edu

***Abstract*—In this paper, the performance criteria, required design, and possible operating modes for IRS at THz frequencies are derived and presented. Due to device constraints, codebooks that can define wavefronts within the near-field may be required for optimal IRS efficiency. Numerical results are provided to benchmark the performance of Bessel beams with conventional beamforming under various communication scenarios, which show that Bessel beam wavefronts have promising applications in next-generation wireless standards at (sub) THz frequencies.**

***Index Terms*—Terahertz communications; Intelligent Reflecting Surfaces; Bessel beams; Beamforming; Reflectarrays**

I. Introduction

Intelligent reflecting surfaces (IRSs) are breakthrough devices proposed to enable programmable wireless environments and improve channel robustness [1]. Thus, these are considered an attractive prospect in enabling Terahertz (THz)-band communications, a front-runner technology for next generation wireless networks [2]. The massive available bandwidth in the THz band ($0.1\,\mathrm{THz}$ to $10\,\mathrm{THz}$) can be utilized to achieve very high data rates and extremely dense networks, neither of which can be supported in the overcrowded portion of the electromagnetic (EM) spectrum currently utilized. However, the very large path losses at THz frequencies, the low power output (a few mW or less per element) of THz signal sources, and the impact of everyday obstacles as opaque barriers to THz signals are significant roadblocks in exploiting the THz band. Further, while sophisticated beamforming antenna arrays could be utilized to partially combat these challenges, it is unlikely that many low-power, low-complexity devices within the dense, interconnected networks of the future will have this capability. Thus the programmable, low-cost, and multi-user capability of an IRS can serve to make THz-band a reality.

IRSs enable wavefront engineering, in which the local phase and amplitude response of an aperture system are manipulated to generate a beam, or wavefront, shaped by the EM superposition of the radiation response of the individual components of the aperture [3]. A well-known example of wavefront engineering is beamforming, where arrays are utilized to produce a directional, planar Gaussian beam in the far-field of the IRS. In this direction, the most important IRS objectives, such as increasing the channel rank and enabling a desired signal to noise ratio (SNR), have been studied under two major assumptions: a) far-field operation of the IRS, and b) dynamic phase control of the IRS elements [4].

However, these assumptions become invalid at THz frequencies due to the device-physics and working principle. More specifically, the far-field operation cannot be considered valid for most scenarios unless the electrical size and, therefore, the gain of the IRS is extremely low - which would defeat the original purpose of the IRS. In the near-field, however, the assumption of regular beamforming no longer holds – the planar Gaussian wavefront is compromised [5]. While near-field signal processing is being investigated both through beamfocusing and customized radiation patterns through metasurfaces [6], [7], the question remains: can we enable enhanced wireless communications and also reduce signal processing demands?

In this paper, we highlight the need for and present alternate wavefronts through generalized codebooks. First, in Sec. II, we present a practical approach to IRS design by explaining and quantizing the required IRS support, in terms of the desired bit error rate (BER) and modulation order, thereby generating accurate estimates on the IRS size, number of elements, and the corresponding far-field distance. In Sec. III, we present the IRS as a phase transformation matrix, explain the wave generation principle, and discuss the assumptions of beamforming that render it inefficient within the near-field. We investigate and evaluate Bessel beams as an alternate mode of IRS-operation in the near-field. We present our results in Sec. IV and conclude our paper in Sec. V.

II. IRS Design and Operation

In this section, we describe the design requirements and operation of the IRS. To adequately contrast the required gain with aperture size, number of elements, and array factor, we consider an IRS designed similarly to antenna arrays, with $\lambda/2$ inter-element spacing, where λ is the free space wavelength at the design frequency. For stringent IRS characterization, we assume the LoS link between the TX and RX as not applicable.

A. IRS Requirements

For a TX-IRS-RX link, the minimum required SNR, S_{min}, in dB, required to sustain a particular data rate is [8]:

$$S_{min} = 10\log_{10}\left(\frac{E_b}{N_0}\frac{f_b}{B}\right) + NF, \tag{1}$$

where f_b refers to the channel bit rate and B refers to the considered bandwidth, and E_b/N_0 is the minimum energy per bit to noise spectral density ratio, derived from the Q-function at the desired BER. NF accounts for the noise factor during demodulation prior to processing. Therefore, the minimum power P_{RX} required at the receiver is [8]:

$$P_{RX} \geq S_{min} + \Xi, \tag{2}$$

where Ξ is the total noise power in dB, dependent on the bandwidth B and the noise power spectral density (PSD) N_0. However, for a given transmitted power P_{TX}, we know that:

$$P_{RX} = P_{TX} - PL + G_{sys}, \tag{3}$$

where PL is the distance dependent path loss, which, over the total distance R from the TX-IRS-RX channel consists of the spreading loss L_S:

$$L_S = 10\log_{10}\left(\frac{(4\pi R)^2}{\lambda^2}\right), \tag{4}$$

and the absorption loss L_{ABS}:

$$L_{ABS} = 10\log_{10}\left(exp(k_{abs}\lambda R)\right), \tag{5}$$

where k_{abs} is the absorption coefficient at the design frequency. G_{sys} in (3) is the combined gain of the system which counters this path loss, and from (2) and (3), we can see there is a minimum threshold. Assuming the TX-IRS and the IRS-RX orientations are optimally setup, for example through cascaded channel estimation [9], G_{sys} must then be met through a combination of the end nodes gain (TX–RX) and the IRS gain. For a given complexity (gain) of the end nodes G_{TX} and G_{RX}, the required IRS gain G_{IRS} can then be derived:

$$G_{IRS} = G_{\text{sys}} - (G_{TX} + G_{RX}). \tag{6}$$

Clearly, the gain of the devices in the system must compensate for higher path losses when the frequencies are greater. Additionally, regardless of the link distance and the carrier frequency, the brunt of the performance criteria must be borne by the IRS for less complex devices. The IRS should then be designed so as to facilitate such high gain requirements, and when feasible, configured to operate at reduced complexity for greater energy efficiency.

B. IRS Design

The required gain from the IRS directly corresponds to an effective aperture size of the IRS, which also allows the designer to ascertain the number of elements in each row and column of the IRS. More specifically, the gain G of a device reduces the beamwidth of the radiated beam by increasing the directivity. Assuming the directivity equal to the gain, the solid radiation angle Ω, is found as:

$$\Omega = \frac{\pi^2}{G}, \tag{7}$$

where the gain is expressed as a linear value (not dB). Then, the required side length L of a square IRS of size $(N \times N)$ is:

$$L = \left(\frac{\lambda}{2\pi}\right)\left(\frac{2.782}{\psi - 1}\right), \tag{8}$$

where $\psi = \sqrt{\Omega}$ is the equivalent beamwidth in the elevation and azimuth planes.The corresponding far-field distance D_{ff} of such a device is [5]:

$$D_{ff} = 2\frac{L^2}{\lambda} = \frac{N^2\lambda}{2}, \tag{9}$$

where, with an inter-element spacing of d, L contains an equivalent number of elements, $N = L/d$. In (9), we assume $d = \lambda/2$, maximizing array aperture and directivity without introducing unwanted grating lobes and spurious effects.

C. IRS Efficiency

Each element of an $M \times N$ IRS receives an incident beam from the TX, implements a phase shift upon it and re-radiates it. Therefore, the SNR value at the RX is the result of the salient features of the system – input power P_{TX}, noise power Ξ, as well as the specific link configurations – path loss PL, IRS size $(M \times N)$, and the codebook $C(\Phi)$ at the IRS. The IRS elements $(m \in M, n \in N)$ are $D^{TX}_{m,n}$ and $D^{RX}_{m,n}$ from the TX and RX respectively. For a given power P_{TX} and noise power Ξ, the obtained SNR at the RX will then be:

$$SNR = \frac{P_T}{\Xi}\left(\sum_{m=0}^{M-1}\sum_{n=0}^{N-1}(PL)e^{-jk(D^{TX}_{m,n}+D^{RX}_{m,n})e^{j\phi_{m,n}}}\right). \tag{10}$$

Here, a correction phase $e^{j\phi_{m,n}}$ is applied through the codebook $C(\Phi)$ across the IRS elements to counter the specific phase difference, $e^{-jk(D^{TX}_{m,n}+D^{RX}_{m,n})}$, resulting from the slightly different path lengths through each IRS element from the TX to the RX, where k is the wave vector. The IRS efficiency is thus a measure of how well $C(\Phi)$ across the IRS compensates for the actual phase differences in the links, the sum total of which governs the reception (transmission) from (to) the TX (RX). We thus define the IRS efficiency factor, EF_{IRS}, as:

$$EF_{IRS} = \frac{\left|\sum_{m=0}^{N-1}\sum_{n=0}^{N-1} e^{-jk(D^t_{m,n}+D^r_{m,n})e^{j\phi_{m,n}}}\right|^2}{M^2N^2}, \tag{11}$$

which completely accounts for the effects of both the TX–IRS and IRS–RX manifestations in the codebook $C(\Phi)$ at the IRS. The maximum value of EF_{IRS} is 1, at highest efficiency. For a square IRS, $M = N$, and (10) can be rewritten as:

$$SNR = \left(\frac{N^2(PL)(P_T)}{\sigma^2}\right)EF_{IRS}, \tag{12}$$

where it is clear that for all other variables held constant, the efficiency factor linearly affects the SNR.

III. Wavefront Generation at the IRS

As shown in Fig. 1a), the IRS intercepts an incident wave and transcribes a desired wavefront on it, through the codebook $C(\Phi)$. Considering a beam traveling in the z-direction, and an IRS in the $x - y$ plane, the definition of the phase

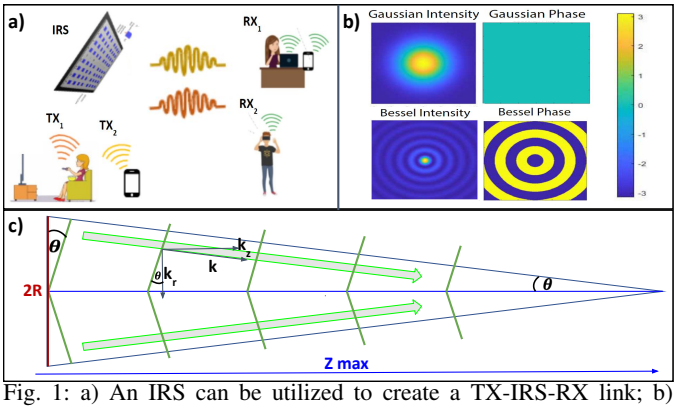

Fig. 1: a) An IRS can be utilized to create a TX-IRS-RX link; b) the utilization of the IRS as a phase transformation matrix enables wavefront engineering and novel beam profiles; and c) the Bessel beam wavefront is analogous to plane waves travelling on a cone.

transformation matrix $M(x, y)$ across the IRS aperture is given as per the Huygens-Fresnel model [10]. Here, EM scalar diffraction theory is utilized to evaluate the complex amplitude $A(x, y, z)$ of the EM wave with a wavevector k at any point from a given field distribution $A(\xi, \eta, 0)$ at an aperture (ξ, η) orthogonal to the wave propagation direction z:

$$A(x, y, z) = \frac{1}{j\lambda}\iint_V A(\xi, \eta, 0)\frac{\exp(-jkr_1)(1 + cos\psi)}{2r_1}d\xi\, d\eta. \quad (13)$$

In (13), $cos\psi$ and r_1 both specify the information about the orientation and distance of the point (x, y, z) from the aperture spot (ξ, η). The complex field $A(\xi, \eta, 0)$ is given as $\S \exp(j\Phi)$, where $\S$ is the magnitude and Φ is the phase through which the IRS response manifests within the resultant complex field in (13). In the discussion that follows, without loss of generality and only for simplicity, we assume that the IRS phase transformation matrix is able to completely capture the incident wave from the TX, and thus discuss the operation of the IRS from an aperture standpoint, focusing on the beam profile as directed towards the RX.

A. Beamforming - A phased array approach

The characteristic approach of beamforming is to simplify the point by point field in (13) instead towards a direction specified through the spherical co-ordinates (θ, ϕ). Then, the codebook across the IRS $C(\Phi)$ is given as [5]:

$$C(\Phi) == -k(d\sin\theta(\Delta x\cos\phi + \Delta y\sin\phi)), \quad (14)$$

with d as the separation between the elements. Setting Δx or Δy to 1 signifies a progression in the x or y direction, respectively. Thus, assuming far-field operation, $C(\Phi)$ attempts to counter the approximate path (and corresponding phase) differences from each IRS element, dependent on the angles of orientations, through a linear progressive phase shift wrapped around 2π radians.

B. Beamfocusing - A lens approach

Beamfocusing requires the exact position of the TX and RX. Here, $C(\Phi)$ is of the form [5]:

$$C(\Phi) = e^{+jkr_1}, \quad (15)$$

providing an exact conjugate of the individual path distance from each element to the RX, with the convergence at a specific spot. The resolution (beam-spot) F governed by the Abbe limit [11], which in an aperture of size R is:

$$F = 1.02\lambda/(R/2). \quad (16)$$

C. Bessel Beams - A hybrid approach

Beamforming requires far-field operation, while beamfocusing produces a specific convergence at a fixed point (no propagation) with exact location requirements. Thus, there is a need to develop a beam where, within the near-field, deterministic propagation and collimation can be fulfilled.

In this light, we investigate Bessel beams, first introduced by Durnin *et. al* in [12]. Their beam profile $B(x, y, z)$ is characterized as:

$$B(x, y, z) = J_l(k_r\sqrt{x^2 + y^2})exp(jk_z z)exp(jl\tan^{-1}(y/x)), \quad (17)$$

where $J_l(\cdot)$ is the l-order Bessel function, k_z and k_r are the transverse and radial wavevectors with $k_z^2 + k_r^2 = k^2$, where k is the wave vector of the beam. Since the Bessel function is distance invariant, these beams are non-diffracting, wherein the time averaged beam intensity is independent of the distance the beam travels. Higher order Bessel beams carry orbital angular momentum (OAM) due to an azimuthal phase, but at present, we restrict our analyses to the zero-th order, or $l = 0$.

True Bessel beams require infinite power [12]. However, quasi-Bessel beams can be setup within a finite propagation distance, as shown in Fig. 1c). The required codebook $C(\Phi)$ mimics plane waves travelling inwards on a cone:

$$C(\Phi) = k\sqrt{x^2 + y^2}sin(\theta), \quad (18)$$

where θ describes the angle of the realized cone. The resultant beam profile is shown in Fig. 1b), wherein a beam characterized by a non-diffracting central spot along the central axis of the so-defined cone, with concentric rings around it, is setup.

The beam dissolves into a diverging ring beyond a maximum distance of propagation Z_{max}, which, for a finite aperture of $2R$, is found as [13]:

$$Z_{max} = \frac{R}{tan(\theta)}, \quad (19)$$

which, due to the geometric relations observable in Fig. 1c) can be approximately modeled as [13]:

$$Z_{max} \approx R\frac{k_z}{k_r} = R\sqrt{(k/k_r)^2 - 1}, \quad (20)$$

thus indicating that for a larger aperture as well as a greater design frequency, the range of the Bessel wavefront increases.

The potential benefits of Bessel beams are that unlike beamforming, these work within the massive near-field and, unlike beamfocusing, are valid across an axis of propagation (the direction of the cone). The gain from the Bessel can be estimated by considering the number of concentric rings that the RX, depending on its size, may receive [13]. The power and information carried in each ring of the Bessel beam, and the central spot size, is the same. Thus, by ensuring that the

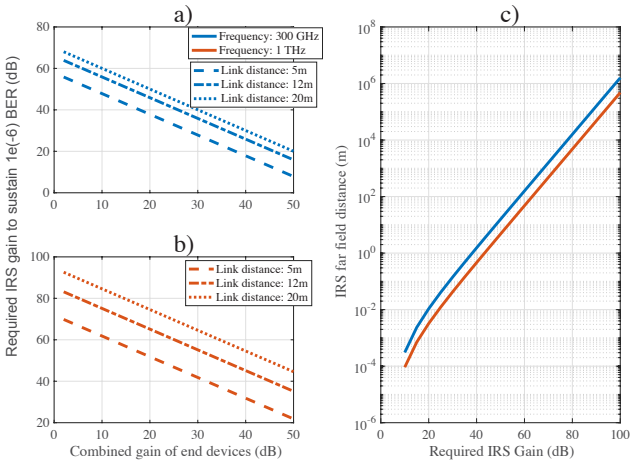

Fig. 2: The relation between the required IRS gain with a changing end-node complexity at: a) 300 GHz; and b) 1 THz. c) The corresponding far-field distance of the IRS.

central spot size is designed to have, at minimum, the power required to meet the link budget from (3), robust performance will be guaranteed. From [13], we note that when the central spot size is chosen to be a, $Z_{max} \approx kRa/2$ and the power, P contained within the central spot is:

$$P = P_T(a/R) \approx P_T \frac{1}{1+4M/3}, \tag{21}$$

where P_T is the total power at the IRS aperture and M is the number of concentric rings, or zeros, of the equivalent Bessel function that can be captured within this aperture. Thus, for communications, a wider central spot increases both the percentage of power within the central spot and the distance over which the Bessel is valid.

IV. Results

In this section, we first present the IRS design requirements as per the discussion from Sec. II, and evaluate the subsequent wavefront characteristics as per the discussion of Sec. III. To characterize the trend across the THz band, we consider two design frequencies of 300 GHz and 1 THz.

A. Required IRS Gain and Size

We present the required gain from the IRS for a changing complexity (gain) of the end nodes to close the communication link at several distances in Fig. 2. We consider a 10 Gbps link, with BPSK modulation (10 GHz bandwidth) and a desired BER of 10^{-6}. The noise PSD is set as per that from the TeraNova testbed at Northeastern University [14] at 10^{-17} W/Hz, with 100 mW transmitted power. As seen in Fig. 2a) and Fig. 2b), regardless of the communication link distance, a greater design frequency requires a larger IRS gain due to increased path loss. The corresponding far-field distance is seen in Fig. 2c); we observe that for the same gain requirement, the far-field distance is smaller at a larger design frequency, and the devastating near-field phenomenon at THz frequencies is due to the very large gain requirement.

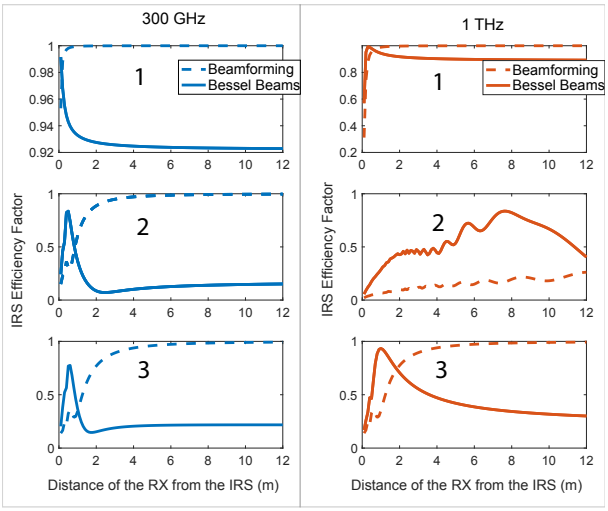

Fig. 3: a) A comparison between the IRS efficiency through beamforming and Bessel at 300 GHz; and b) 1 THz. The scenarios considered are as per the parameters of Table I.

B. Wavefront Response

To characterize the wavefront efficiency through (11), we specify the IRS size and other parameters by considering three operating scenarios:

- Scenario 1: TX-RX pair designed similarly (maximum gain with a physical size of 1 mm), regardless of design frequency.
- Scenario 2: The RX is considered as a unitary gain device.
- Scenario 3: The far-field distance of the IRS is fixed to 12 m, at the limit of most indoor communication scenarios, regardless of design frequency.

The corresponding values are presented in Table I. The spot size of the Bessel beam is designed to be 10 times the RX size, or 10 mm, to ensure SNR requirements are always fulfilled.

We present the comparison between Bessel and beamforming efficiency from (13) for (11) in Fig. 3a) and Fig. 3b), for the two design frequencies, with the three respective scenarios highlighted. The RX is assumed to be along the central axis of the IRS. In both Fig. 3a) and Fig. 3b), for scenario 1, the IRS is extremely small. Thus, both Bessel and beamforming beams are nearly equal in their application, and beamforming quickly converges to the ideal.

However, under Scenario 2, the IRS is massive at 1 THz (see Table I. Indeed, in Fig. 3b), we observe that while the beamforming efficiency is crippled, the range of the Bessel increases substantially. The improvement is more pronounced for the larger design frequency, as Bessel beams work better at higher frequencies, an advantage for THz communications.

Further, as expected from the results of Scenario 3, we observe that regardless of the design frequency, beamforming efficiency improves similarly for the same far-field.

We note that the simulated Bessel range in Fig. 3a) and Fig. 3b) does not exactly match the theoretical values highlighted in Table I. This is due to the fact that we create a Bessel beam by implementing a conical phase on a plane

TABLE I: Required IRS Size (N × N elements), Far-Field Distance and Bessel Propagation Distance

Scenario	Design Frequency									
	300 GHz					1 THz				
	TX–RX Gain	IRS Gain	N	Far-field	Z_{max}	TX–RX Gain	IRS Gain	N	Far-field	Z_{max}
1	31.96 dB	32.26 dB	23	0.24 m	0.1436 m	52.84 dB	44.4 dB	93	1.27 m	0.6008 m
2	16.98 dB	47.24 dB	129	8.17 m	0.8354 m	27.42 dB	69.83 dB	1747	457.17 m	11.4096 m
3	N.A.	48.83 dB	156	12 m	1.005 m	N.A.	54.01 dB	283	12 m	1.8352 m

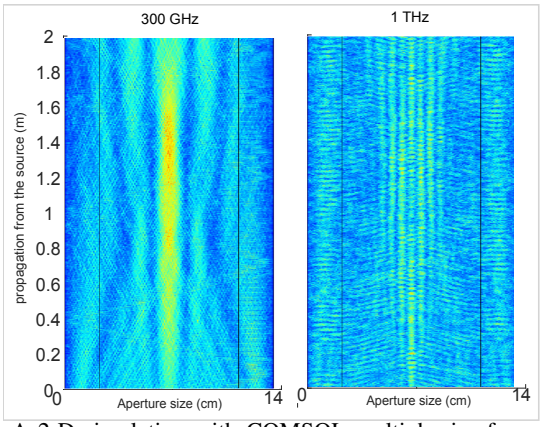

Fig. 4: A 2-D simulation with COMSOL multiphysics for a 10 cm aperture Axicon, indicating that the response from the IRS is close to an ideal Bessel.

wave, rather than simply assuming the perfect Bessel function at the aperture. Nonetheless, the resultant beam resembles Bessel beams, as evidenced by the full-wave simulations for the two design frequencies presented in Fig. 4. Here, an 8 degree conical phase on a 10 cm aperture (size limited due to computational complexity) is utilized and the resulting EM wave is evaluated through COMSOL Multiphysics. It is observed that the same Bessel like structure, with a central bright spot and concentric rings is formed for both frequencies, with a larger propagation range and more concentric rings at the larger design frequency.

V. Conclusions

In this paper, we have highlighted the need for novel wavefronts in IRS deployments at THz frequencies, where electrically large devices with massive far-field regions are expected. In the operating near-field, beamforming could be compromised. We thus envision new wavefronts with a defined propagation axis (similar to beamforming in the far-field) which can be generated through a generalized codebook.

Our results indicate that Bessel beams could serve the envisioned wavefront characteristics. The design relation between the Bessel beam central spot size width and power, the IRS aperture size, and the maximum propagation distance are generalized expressions. The desired angle of the central axis of propagation is sufficient to characterize the RX direction; thus, all the algorithms developed for beam-alignment in conventional beamforming could potentially be applicable to Bessel beams as well. In this light, we consider Bessel beams a promising contender for the 'ideal' wavefront in the near-field employed in next generation of wireless communications, even as we continue to explore customized wavefronts. Nonetheless, IRS design and performance considerations must be closely complemented with the manifestations on IRS efficiency.

References

[1] M. Di Renzo, M. Debbah, D.-T. Phan-Huy, A. Zappone, M.-S. Alouini, C. Yuen, V. Sciancalepore, G. C. Alexandropoulos, J. Hoydis, H. Gacanin *et al.*, "Smart radio environments empowered by reconfigurable ai meta-surfaces: An idea whose time has come," *EURASIP Journal on Wireless Communications and Networking*, vol. 2019, no. 1, pp. 1–20, 2019.

[2] T. S. Rappaport, Y. Xing, O. Kanhere, S. Ju, A. Madanayake, S. Mandal, A. Alkhateeb, and G. C. Trichopoulos, "Wireless communications and applications above 100 GHz: Opportunities and challenges for 6G and beyond," *IEEE Access*, vol. 7, pp. 78 729–78 757, 2019.

[3] D. Headland, Y. Monnai, D. Abbott, C. Fumeaux, and W. Withayachumnankul, "Tutorial: Terahertz beamforming, from concepts to realizations," *Apl Photonics*, vol. 3, no. 5, p. 051101, 2018.

[4] J. Zhao, "A survey of intelligent reflecting surfaces (irss): Towards 6g wireless communication networks," *arXiv preprint arXiv:1907.04789*, 2019.

[5] C. A. Balanis, *Antenna theory: analysis and design*. John Wiley & Sons, 2016.

[6] C. Liaskos, S. Nie, A. Tsioliaridou, A. Pitsillides, S. Ioannidis, and I. Akyildiz, "A novel communication paradigm for high capacity and security via programmable indoor wireless environments in next generation wireless systems," *Ad Hoc Networks*, vol. 87, pp. 1–16, 2019.

[7] K. Dovelos, S. D. Assimonis, H. Q. Ngo, B. Bellalta, and M. Matthaiou, "Intelligent reflecting surfaces at terahertz bands: Channel modeling and analysis," *arXiv preprint arXiv:2103.15239*, 2021.

[8] A. Goldsmith, *Wireless communications*. Cambridge university press, 2005.

[9] P. Wang, J. Fang, H. Duan, and H. Li, "Compressed channel estimation for intelligent reflecting surface-assisted millimeter wave systems," *IEEE Signal Processing Letters*, vol. 27, pp. 905–909, 2020.

[10] F. Depasse, M. Paesler, D. Courjon, and J. Vigoureux, "Huygens–fresnel principle in the near field," *Optics letters*, vol. 20, no. 3, pp. 234–236, 1995.

[11] E. Abbe, "Contributions to the theory of the microscope and microscopic perception," *Archive for microscopic anatomy*, vol. 9, no. 1, pp. 413–468, 1873.

[12] J. Durnin, "Exact solutions for nondiffracting beams. I. the scalar theory," *JOSA A*, vol. 4, no. 4, pp. 651–654, 1987.

[13] J. Durnin, J. Miceli, and J. H. Eberly, "Comparison of bessel and gaussian beams," *Optics letters*, vol. 13, no. 2, pp. 79–80, 1988.

[14] P. Sen, V. Ariyarathna, A. Madanayake, and J. M. Jornet, "Experimental wireless testbed for ultrabroadband terahertz networks," in *Proceedings of the 14th International Workshop on Wireless Network Testbeds, Experimental evaluation & Characterization*, 2020, pp. 48–55.